BRIEF COMMUNICATION
https://doi.org/10.1038/s41592-021-01078-7

nature methods

A fast, high-affinity fluorescent serotonin biosensor engineered from a tick lipocalin

Shen Zhang[1,2,3,6], Xinyu Li[1,2,6], Shengyu Zhao[1,3], Mikhail Drobizhev[4] and Hui-wang Ai[1,2,3,5] ✉

Serotonin (5-HT) is an important signaling monoamine and neurotransmitter. We report structure-guided engineering of a green fluorescent, genetically encoded serotonin sensor (G-GESS) from a 5-HT-binding lipocalin in the soft tick *Argas monolakensis*. G-GESS shows fast response kinetics and high affinity, specificity, brightness and photostability. We used G-GESS to image 5-HT dynamics in cultured cells, brain slices and behaving mice.

5-HT is a key neurotransmitter modulating mood, anxiety, appetite, sleep, sexuality, learning and memory, and is a key hormone in peripheral tissues regulating a large array of processes, including gastrointestinal motility, hematopoiesis, vasoconstriction, insulin secretion and glucose metabolism[1]. Serotonergic dysregulation has been linked to various pathological conditions, such as depression, schizophrenia, diabetes, obesity and cardiovascular disorders[1]. A further understanding of 5-HT signaling, as well as the development of corresponding disease intervention strategies, requires the ability to monitor 5-HT dynamics in biological systems with high specificity and spatiotemporal precision[1,2].

Microdialysis and fast-scan cyclic voltammetry have been used widely to follow 5-HT dynamics, but are limited in temporal resolution, spatial precision and/or chemical selectivity[3,4]. Although several chemically synthesized fluorescent sensors have been reported[5,6], achieving long-term, cell-specific and minimally invasive imaging of 5-HT in vivo remains a challenge. Thus, there is a great interest to develop genetically encoded 5-HT biosensors[2].

Microbial periplasmic binding proteins (PBPs) or G-protein coupled receptors (GPCRs) have been fused with circularly permuted green fluorescent protein (cpGFP) to create biosensors typically expressed at the cell surface to detect secreted neurotransmitters and neuromodulators[2]. Although it would be possible to develop similar biosensors for 5-HT from PBPs or GPCRs, we chose to investigate additional 5-HT-binding proteins for several reasons. First, natural 5-HT binding PBPs have not been identified, and it is challenging to re-engineer a PBP to accommodate 5-HT and simultaneously achieve suitable specificity and affinity. Also, GPCR-based biosensors often respond to all molecules that interact with the parental GPCRs, resulting in artifacts when GPCR antagonists or agonists are used concurrently[7]. Furthermore, GPCR-based biosensors may suffer from slow dissociation kinetics[7], and overexpression of GPCRs may perturb cell signaling, which is highly organized and tightly controlled[8].

Blood-feeding arthropods can release soluble, monoamine-binding lipocalin proteins to the feeding site of their hosts to neutralize host inflammatory responses and prevent blood clotting, platelet aggregation and vasoconstriction[9]. We reasoned that these small (17 kDa) and monomeric lipocalins could be explored to develop biosensors. Moreover, the ability to express these proteins in a soluble format in *Escherichia coli* should facilitate high-throughput screening and sensor characterization. Furthermore, these proteins are not naturally expressed in common model organisms, thereby minimizing the interference of derived biosensors with endogenous signaling.

In a literature survey, we identified AM182 from the soft tick *Argas monolakensis* and D7r4 from the mosquito *Anopheles gambiae* as promising candidates because of their high affinity to 5-HT and the availability of protein structures[9,10]. We reasoned that insertion of cpGFP into these proteins at locations undergoing substantial structural rearrangement upon ligand binding may result in allosteric coupling of ligand binding to cpGFP fluorescence (Fig. 1a). We thus analyzed 5-HT-dependent changes in dihedral angle (defined by the C_α atoms spanning every four sequential residues) on the basis of ligand-bound and ligand-free protein structures. The apo and bound structures of D7r4 were both reported, whereas the structure of AM182 was available only in the 5-HT-bound state[9]. Therefore, we analyzed dihedral angle changes for AM10, a histamine-binding protein homologous to AM182, and identified loops 4, 5 and 9 as promising insertion sites (Extended Data Fig. 1a–c). Similarly, we identified loop 2 of D7r4 for possible cpGFP insertion (Extended Data Fig. 1d–f).

We next experimentally inserted cpGFP into the identified loops. Insertion at loop 9 of AM182 generated a prototypic 5-HT biosensor (G-GESS0.1) showing 5-HT-induced fluorescence increase of 10%, whereas other insertion sites led to variants that were either unresponsive or nonspecifically responsive to 5-HT. Through multiple rounds of directed evolution from G-GESS0.1 (Extended Data Fig. 2), we derived G-GESS with an overall 12-fold excitation–ratiometric response (R/R_0, where R is the ratio of fluorescence at 480 nm to that at 400 nm) to 5-HT and nearly 600% ($\Delta F/F_0$) intensiometric fluorescence increase near its major absorbance peak at ~500 nm (Fig. 1a,b).

When saturated with 5-HT, the intrinsic brightness of G-GESS under one-photon excitation is ~70% of enhanced green fluorescent protein (EGFP) (Supplementary Table 1). G-GESS has a broad two-photon excitation with high brightness and large response between 880 and 990 nm (Supplementary Table 1 and Extended Data Fig. 3). We further tested the specificity of G-GESS against a panel of additional neurotransmitters and other relevant molecules, and none of these compounds elicited a noticeable fluorescence change at physiologically relevant concentrations (Fig. 1c). Titrating G-GESS with 5-HT revealed a dissociation constant (K_d) of ~43 nM with > 5×10^5-fold selectivity over structurally similar

[1]Center for Membrane and Cell Physiology, University of Virginia, Charlottesville, VA, USA. [2]Department of Molecular Physiology and Biological Physics, University of Virginia, Charlottesville, VA, USA. [3]Department of Chemistry, University of Virginia, Charlottesville, VA, USA. [4]Department of Microbiology and Immunology, Montana State University, Bozeman, MT, USA. [5]The UVA Cancer Center, University of Virginia, Charlottesville, VA, USA. [6]These authors contributed equally: Shen Zhang, Xinyu Li. ✉e-mail: huiwang.ai@virginia.edu

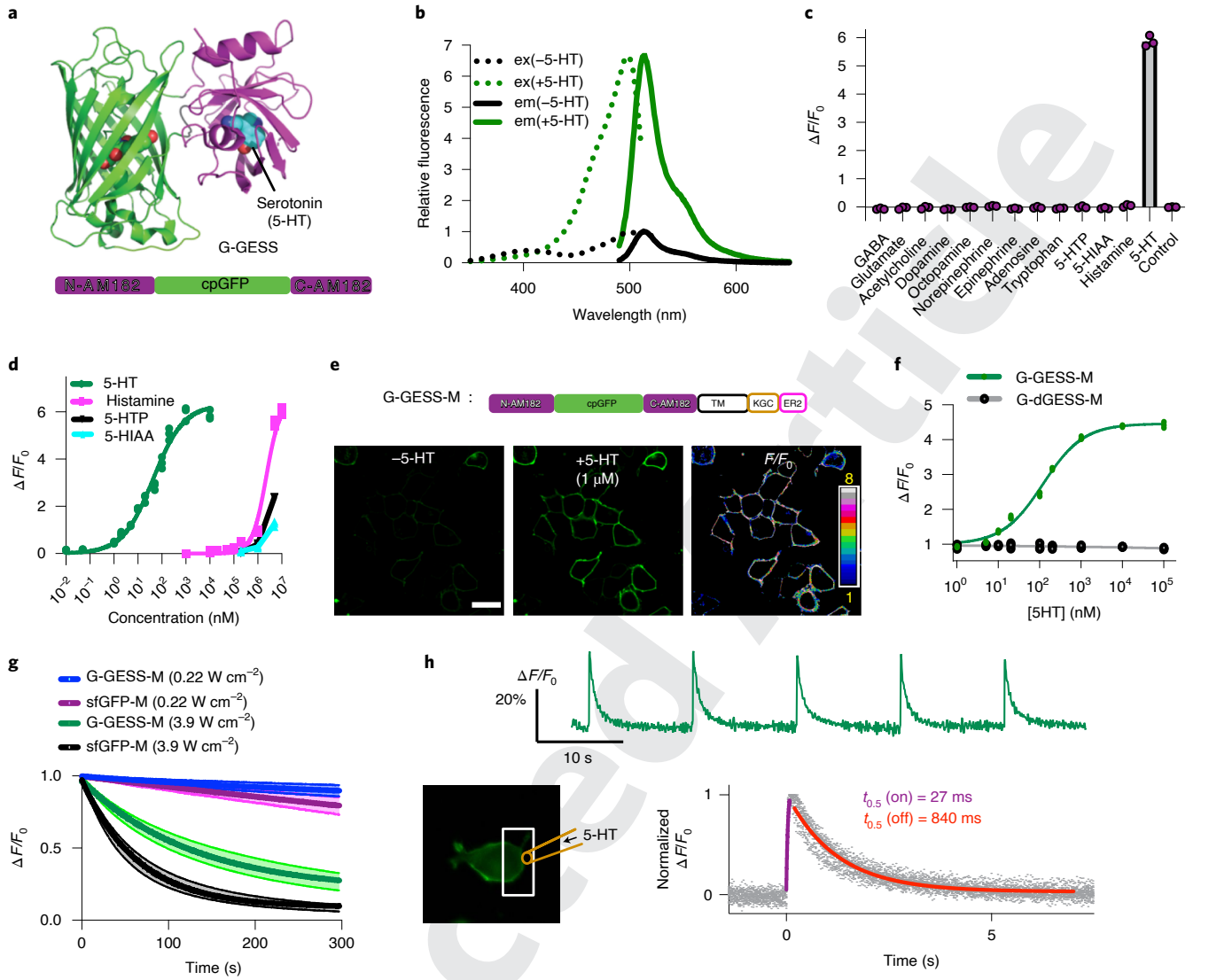

Fig. 1 | Design and characterization of G-GESS. a, Schematic representation of G-GESS, showing insertion of cpGFP (green) into loop 9 of AM182 (magenta). **b**, Excitation (dotted line) and emission (solid line) spectra of purified G-GESS in the presence (green) or absence (black) of 10 μM 5-HT. Spectra were normalized to the maximal fluorescence of G-GESS in the absence of 5-HT. **c**, Fluorescence of G-GESS in response to the indicated neurotransmitters and other relevant substances (10 μM 5-HT and 100 μM of other molecules); $n = 3$ for each group. GABA, gamma-aminobutyric acid. **d**, Dose-response curve of purified G-GESS for 5-HT ($K_d = 43 \pm 5$ nM), histamine ($K_d = 2.3 \pm 0.4$ mM), 5-HTP ($K_d > 5$ mM) and 5-HIAA ($K_d > 5$ mM); $n = 3$ for each group. **e**, Top: domain arrangement of G-GESS-M, showing a C-terminal PDGFRβ TM domain, a Kir2.1-derived Golgi export trafficking signal (KGC) and an ER export signal (ER2). Bottom: representative fluorescence and pseudocolor ratiometric images of G-GESS-M at the surface of HEK 293T. This experiment was repeated three times with similar results using independent cultures. Scale bar, 20 μm. **f**, 5-HT dose-response curve of G-GESS-M ($K_d = 120 \pm 8$ nM) and G-dGESS-M at the surface of HEK 293T; $n = 3$ wells of cells per group with 10^5 cells per well. **g**, Photobleaching of G-GESS-M and sfGFP-M at the surface of HEK 293T on a wide-field microscope at the two indicated light intensity levels ($t_{1/2} = 123$ s for G-GESS-M and 50 s for sfGFP-M at 3.9 W cm^{-2}). Data are presented as mean ± s.d. ($n = 18$ cells from three independent cultures for each group). **h**, Analysis of G-GESS-M kinetics by puff application of 1 μM 5-HT. A representative trace for five sequential applications of 5-HT to a single cell is shown at the top. Presented at the bottom are normalized data points for 25 repeats (five single cells with five applications each) fitted for exponential growth and decay.

molecules such as histamine, 5-hydroxyindoleacetic acid (5-HIAA) and 5-hydroxytryptophan (5-HTP) (Fig. 1d).

To anchor G-GESS to the cell surface, we fused it to a platelet-derived growth factor receptor beta (PDGFRβ) transmembrane (TM) domain and Kir2.1-derived Golgi (KGC) and ER export (ER2) signals (hereafter referred to as G-GESS-M) (Fig. 1e and Supplementary Fig. 1)[11]. G-GESS-M localized to the surface of HEK 293T cells (Extended Data Fig. 4). It displayed ~350% ($\Delta F/F_0$) fluorescence increase in response to 5-HT with a K_d of ~120 nM, and better photostability than superfolder GFP (sfGFP) (Fig. 1e–g). We next monitored the sensor's response to a local application of 5-HT (1 μM) and determined the half-time ($t_{0.5}$) for association and spontaneous dissociation to be 27 ms and 840 ms, respectively (Fig. 1h). Furthermore, we introduced two mutations into G-GESS-M to generate an unresponsive control, G-dGESS-M (Extended Data Fig. 5).

We used G-GESS-M to monitor physiological 5-HT dynamics. 5-HT is synthesized and released from pancreatic β-cells to modulate insulin secretion and islet function[12]. We expressed G-GESS-M in mouse MIN6 β-cells and observed ~25% fluorescent increase triggered by high glucose concentrations (Extended Data Fig. 6a,b).

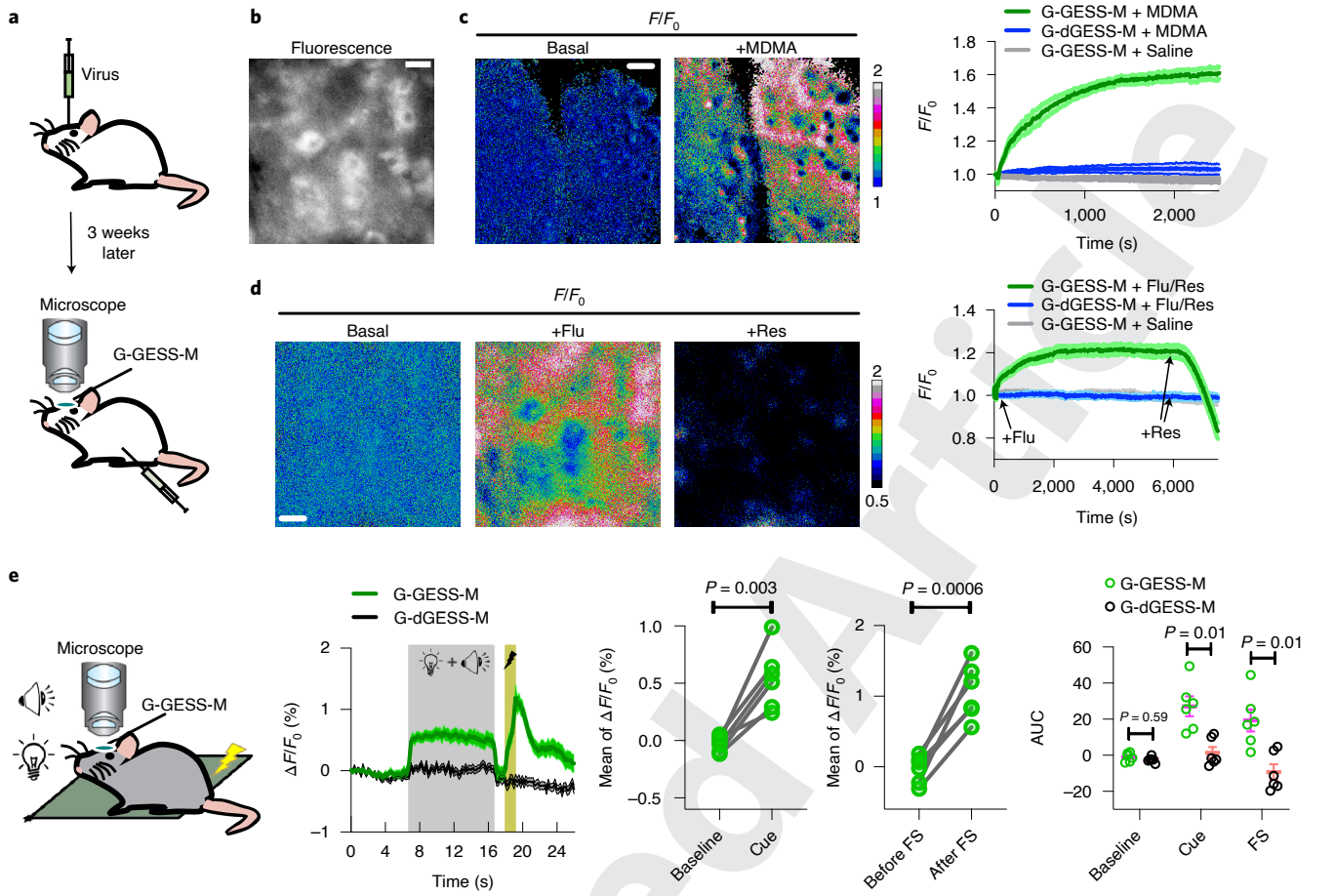

Fig. 2 | Imaging of endogenous 5-HT dynamics with G-GESS in mice. a, Schematic diagram illustrating viral expression and in vivo imaging of G-GESS-M in the PFC of head-fixed mice. **b**, Representative in vivo fluorescence image of G-GESS-M under one-photon microscopy. Scale bar, 20 μm. **c**, Representative ratiometric images and average intensity traces upon MDMA (10 mg kg^{-1}, i.p.) administration. G-dGESS-M and saline injection were used as control groups. Data are presented as mean ± s.e.m.; (n = 3 mice for each group). Scale bar, 20 μm. **d**, Representative ratiometric images and average intensity traces after fluvoxamine (Flu, 2 mg kg^{-1}, i.p.) and reserpine (Res, 0.2 mg kg^{-1}, i.p.) treatments. Data are presented as mean ± s.e.m.; (n = 3 mice for each group). Scale bar, 20 μm. **e**, Responses of G-GESS-M or G-dGESS-M in the PFC during a fear conditioning paradigm consisting of a 10-s audiovisual cue followed by a 1-s break and a 1-s aversive FS. The gray and yellow boxes indicate the time windows for the delivery of cue and 1-s FS, respectively; n = 6 mice (each animal with 15 single trials) for each group. Comparisons of fluorescence responses (mean of $\Delta F/F_0$ for individual G-GESS animals) between baseline (0–7 s) and cue (7–17 s), and between a 1-s timewindow before and after FS. P values determined by paired two-tailed Student's t-tests. Areas under the curve (AUC) for G-GESS and G-dGESS animals during 0–7 s (Baseline), 7–17 s (Cue) and 18–26 s (FS). P values determined by 2-way analysis of variance (ANOVA) with Sidak's multiple comparisons test. Data are presented as mean ± s.e.m.

Furthermore, we expressed G-GESS-M in SH-SY5Y neuroblastoma cells and primary mouse neurons and imaged 5-HT secretion in response to nonivamide, which is a chemical known to induce serotonin release[13], and membrane polarization induced by high potassium concentrations, respectively (Extended Data Fig. 6c,d and Extended Data Fig. 7). In contrast to G-GESS-M, G-dGESS-M was unresponsive under these conditions. To evaluate potential neurotoxicity of G-GESS-M, we compared viability and depolarization-induced Ca^{2+} mobilization of primary mouse neurons expressing cell-membrane-anchored G-GESS or sfGFP and observed no difference (Extended Data Fig. 8)

We expressed G-GESS-M in the hippocampal CA1 region of mouse brains via lentivirus or adeno-associated virus (AAV) transduction and prepared acute brain slices (Extended Data Fig. 9a,b). We detected up to 35% fluorescence increase with excellent signal-to-noise ratio following extracellular field stimulation. The kinetics and magnitude of the responses were dependent on stimulation voltage and frequency (Extended Data Fig. 9c–f). In contrast, we observed no fluorescence change for G-dGESS-M brain slices stimulated in the same manner.

Next, we expressed G-GESS-M in the prefrontal cortex (PFC) of live mice and administered intraperitoneal (i.p.) methylenedioxymethamphetamine (MDMA), a compound known to stimulate, although nonselectively, the release of 5-HT in the brain[14]. We imaged the fluorescence of G-GESS through a pre-installed cranial imaging window and observed a robust ~60% fluorescence increase (Fig. 2a–c). Similarly, we examined the response of G-GESS-M to fluvoxamine (Flu), a selective serotonin reuptake inhibitor. Flu evoked an increase of G-GESS-M fluorescence, which can be reversed by reserpine (Res), a vesicular monoamine transporter inhibitor depleting extracellular 5-HT (Fig. 2d). G-dGESS-M or injection of saline resulted in no obvious response under these conditions.

Previous studies have linked the PFC to fear memory, and cortical 5-HT is expected to increase under fear and stress[15,16]. We thus expressed G-GESS-M in the mouse PFC and used a fear

conditioning paradigm to induce endogenous 5-HT changes (Fig. 2e). We presented mice with an audiovisual cue followed by a break and an aversive footshock (FS). We trained the mice to associate the cue with the aversive signal. During imaging, we observed a robust fluorescence increase in response to the cue, while the following FS stimulation evoked an even higher response which diminished within a few seconds. Control G-dGESS-M mice did not exhibit similar responses, except for a small signal rise during the presentation of the visual cue, which slightly increases the background of fluorescence imaging. These results collectively suggest that G-GESS can detect physiological 5-HT transients in response to behavioral stimuli.

Finally, we used G-GESS-M to monitor pharmacological manipulation of 5-HT synthesis. To normalize fluorescence for varied sensor expression levels, we bicistronically co-expressed G-GESS-M with a red fluorescent protein, mScarlet-I (ref. [17]) (Extended Data Fig. 10a–c) in the mouse hippocampus. We then administered *p*-chlorophenylalanine methyl ester (PCPA) (ref. [18]), a tryptophan hydroxylase inhibitor, for five consecutive days. As expected, we observed a decrease of the green-to-red fluorescence ratio in PCPA-treated mice, while there was no change in mice untreated with PCPA (Extended Data Fig. 10d–f).

In summary, we developed a biosensor suitable for imaging physiological 5-HT dynamics in cell culture, acute brain slices and live mice. Since 5-HT plays important roles both within and beyond the central nervous system (CNS), we expect G-GESS to enable a large array of studies. Because intrinsically G-GESS is not a membrane protein, we envision that G-GESS or its future derivatives can be targeted to intracellular subdomains to monitor 5-HT. Furthermore, in comparison to PBP- or GPCR-based 5-HT biosensors resultant from recent, parallel efforts in other laboratories[19,20], the small size of G-GESS should facilitate the potential use of viral vectors, often with limited packaging capacities, to deliver multiple genes. In addition, diverse lipocalins exist in nature[21] and the lipocalin scaffold has been exploited in laboratories for engineering antibody mimetics[22]. Therefore, there is a potential to expand lipocalin-derived fluorescent biosensors to report on other bioactive compounds.

Online content

Any methods, additional references, Nature Research reporting summaries, source data, extended data, supplementary information, acknowledgements, peer review information; details of author contributions and competing interests; and statements of data and code availability are available at https://doi.org/10.1038/s41592-021-01078-7.

Received: 15 April 2020; Accepted: 25 January 2021;
Published online: 25 February 2021

References

1. Berger, M., Gray, J. A. & Roth, B. L. The expanded biology of serotonin. *Annu. Rev. Med.* **60**, 355–366 (2009).
2. Sabatini, B. L. & Tian, L. Imaging neurotransmitter and neuromodulator dynamics in vivo with genetically encoded indicators. *Neuron* **108**, 17–32 (2020).
3. Chefer, V. I., Thompson, A. C., Zapata, A. & Shippenberg, T. S. Overview of brain microdialysis. *Curr. Protoc. Neurosci.* **Chapter 7**, Unit 7.1 (2009).
4. Puthongkham, P. & Venton, B. J. Recent advances in fast-scan cyclic voltammetry. *Analyst* **145**, 1087–1102 (2020).
5. Jeong, S. et al. High-throughput evolution of near-infrared serotonin nanosensors. *Sci. Adv.* **5**, eaay3771 (2019).
6. Hettie, K. S. & Glass, T. E. Turn-on near-infrared fluorescent sensor for selectively imaging serotonin. *ACS Chem. Neurosci.* **7**, 21–25 (2016).
7. Borden, P. M. et al. A fast genetically encoded fluorescent sensor for faithful in vivo acetylcholine detection in mice, fish, worms and flies. Preprint at *bioRxiv* https://doi.org/10.1101/2020.04.18.048397 (2020).
8. Tubio, M. R. et al. Expression of a G protein-coupled receptor (GPCR) leads to attenuation of signaling by other GPCRs: experimental evidence for a spontaneous GPCR constitutive inactive form. *J. Biol. Chem.* **285**, 14990–14998 (2010).
9. Mans, B. J., Ribeiro, J. M. & Andersen, J. F. Structure, function, and evolution of biogenic amine-binding proteins in soft ticks. *J. Biol. Chem.* **283**, 18721–18733 (2008).
10. Mans, B. J., Calvo, E., Ribeiro, J. M. & Andersen, J. F. The crystal structure of D7r4, a salivary biogenic amine-binding protein from the malaria mosquito *Anopheles gambiae*. *J. Biol. Chem.* **282**, 36626–36633 (2007).
11. Hofherr, A., Fakler, B. & Klöcker, N. Selective Golgi export of Kir2.1 controls the stoichiometry of functional Kir2.x channel heteromers. *J. Cell Sci.* **118**, 1935–1943 (2005).
12. Cataldo Bascuñan, L. R., Lyons, C., Bennet, H., Artner, I. & Fex, M. Serotonergic regulation of insulin secretion. *Acta Physiol. (Oxf.)* **225**, e13101 (2019).
13. Rohm, B. et al. Nonivamide, a capsaicin analog, increases dopamine and serotonin release in SH-SY5Y cells via a TRPV1-independent pathway. *Mol. Nutr. Food Res.* **57**, 2008–2018 (2013).
14. Fletcher, P. J., Korth, K. M., Robinson, S. R. & Baker, G. B. Multiple 5-HT receptors are involved in the effects of acute MDMA treatment: studies on locomotor activity and responding for conditioned reinforcement. *Psychopharmacol. (Berl.)* **162**, 282–291 (2002).
15. Bauer, E. P. Serotonin in fear conditioning processes. *Behav. Brain Res.* **277**, 68–77 (2015).
16. Fujino, K. et al. Increased serotonin release in mice frontal cortex and hippocampus induced by acute physiological stressors. *Neurosci. Lett.* **320**, 91–95 (2002).
17. Bindels, D. S. et al. mScarlet: a bright monomeric red fluorescent protein for cellular imaging. *Nat. Methods* **14**, 53–56 (2017).
18. Paxinos, G., Burt, J., Atrens, D. M. & Jackson, D. M. 5-hydroxytryptamine depletion with para-chlorophenylalanine: effects on eating, drinking, irritability, muricide and copulation. *Pharmacol. Biochem. Behav.* **6**, 439–447 (1977).
19. Unger, E. K. et al. Directed evolution of a selective and sensitive serotonin sensor via machine learning. *Cell* **183**, 1986–2002.e1926 (2020).
20. Wan, J. et al. A genetically encoded GRAB sensor for measuring serotonin dynamics. Preprint at *bioRxiv* https://doi.org/10.1101/2020.02.24.962282 (2020).
21. Flower, D. R., North, A. C. & Sansom, C. E. The lipocalin protein family: structural and sequence overview. *Biochim. Biophys. Acta* **1482**, 9–24 (2000).
22. Skerra, A. Alternative binding proteins: anticalins - harnessing the structural plasticity of the lipocalin ligand pocket to engineer novel binding activities. *FEBS J.* **275**, 2677–2683 (2008).

Methods

Key materials and general methods. pCMV(MinDis).iGluSnFR (Addgene plasmid catalog no. 41732) (ref. [23]), pAAV-hSyn-CheRiff-eGFP (Addgene plasmid catalog no. 51697) (ref. [24]), pLenti-ReaChR-Citrine (Addgene plasmid catalog no. 50956) (ref. [25]) and pCMV-R-GECO1 (Addgene Plasmid catalog no. 32444) (ref. [26]) were gifts from Loren Looger (HHMI Janelia Research Campus), Adam Cohen (Harvard), Roger Tsien (UC San Diego) and Robert Campbell (University of Alberta), respectively. pAdDeltaF6 (Addgene plasmid catalog no. 112867) and pAAV2/9n (Addgene plasmid catalog no. 112865) were gifts from James M. Wilson (University of Pennsylvania). pMD2G (Addgene plasmid catalog no. 12259) and psPAX2 (Addgene plasmid catalog no. 12260) were gifts from Didier Trono (EPFL). All animal procedures were conducted in accordance with the protocol approved by the Animal Care and Use Committee at the University of Virginia. Mice were hosted in a temperature-controlled room (~23 °C) with a 12 h–12 h dark–light cycle and ~50% humidity. SDS-polyacrylamide gel electrophoresis (PAGE) was used to verify the purity of the prepared proteins (Supplementary Fig. 2). Other general information is available from the Reporting Summary.

Library design, construction and screening. We followed a procedure previously reported by Marvin et al.[27] to analyze dihedral angle changes and identify promising sites in AM182 and D7r4 for cpGFP insertion. Next, a cpGFP fragment previously used to develop a genetically encoded H_2S sensor[28] was amplified and inserted to the pre-identified sites using overlap polymerase chain reaction (PCR). The product was cloned into a pTorPE plasmid[26] between *Sal*I and *Hin*dIII restriction sites for bacterial periplasmic expression. To generate gene libraries, overlap PCR and oligonucleotides containing degenerate codons (NNK) were used to randomize residues on the linkers between cpGFP and AM182 fragments, whereas error-prone PCR was used to randomize the whole sensor gene. The resultant libraries were subjected to *E. coli* colony-based screening. Colonies were imaged before and after spraying a fine mist of 100 μM serotonin using a previously described setup[29]. Colonies exhibiting changes in fluorescence intensity was identified using an image processing method described by Kardash et al.[30]. Selected clones were cultured individually in 1.8 ml of liquid Luria-Bertani (LB) medium supplemented with 0.02% L-arabinose and 200 μg ml^{-1} ampicillin with 250 r.p.m. shaking at room temperature for 48 h. Cell lysates were then prepared from bacterial pellets using a laboratory-made solution containing 0.5% octyl glucoside, 0.1 mg ml^{-1} chicken egg lysozyme and 0.2 U ml^{-1} Benzonase in 20 mM Tris-HCl, pH 8. A BioTek Synergy Mx microplate reader was next used to test the responses of cell lysates to 10 μM serotonin. Promising clones were selected for further characterization or another round of protein engineering.

Protein purification and one-photon spectroscopic characterization. G-GESS in pTorPE was cloned into pBAD/His B and used to transform *E. coli* DH10B cells. Protein expression and Ni-NTA based protein purification were performed as previously described[31]. Proteins eluted from Ni-NTA beads were subjected to size-exclusion chromatography through a HiPrep Sephacryl S-200 HR gel filtration column (GE Healthcare) by using an elution buffer containing 100 mM NaCl and 50 mM Tris-HCl, pH 7.4. Resultant proteins were further diluted with the aforementioned elution buffer to a final concentration of ~100 nM and used for protein-based assays, including one-photon spectroscopy, selectivity and binding affinity determination, on a monochromator-based BioTek Synergy Mx plate reader. The peak extinction coefficients and fractional concentrations of the neutral and anionic forms of G-GESS were obtained by following the changes in one-photon absorption spectra (measured with Lambda 950 spectrophotometer, Perkin-Elmer) upon gradual stepwise alkaline titration by following a previously described protocol[32]. Fluorescence quantum yields of anionic forms were measured in dilute solutions (optical density (OD) < 0.1) with an absolute method, using Quantaurus-QY (Hamamatsu) integrating sphere fluorimeter by scanning the blue part of absorption peak with a 5-nm step.

Two-photon spectral characterization. Our experimental setup for two-photon spectral measurements includes a tunable femtosecond laser InSight DeepSee Dual (Spectra Physics) coupled with a photon counting spectrofluorimeter PC1 (ISS). The two-photon fluorescence excitation (2PE) spectra were measured by automatically stepping laser wavelength and recording total fluorescence intensity at each step. The detailed description of the experimental setup and measurement protocol has been presented previously[33]. To scale the two-photon excitation spectra, we define a parameter called two-photon molecular brightness $F_2(\lambda)$. This parameter depends on excitation wavelength λ. Usually, absorption spectra (both one- and two-photon) of cpGFP-based sensors consist of two spectral bands: one for the neutral GFP chromophore (subscript N in the following), and another for the anionic GFP chromophore (subscript A in the following). The two forms coexist in equilibrium with the relative fractional concentrations ρ_N and ρ_A ($\rho_N+\rho_A=1$) that can change upon binding a ligand. The $F_2(\lambda)$ value can be presented as follows: $F_2(\lambda)=\rho_A\varphi_A\sigma_{2,A}(\lambda)+\rho_N\varphi_N\sigma_{2,N}(\lambda)$, where φ is the fluorescence quantum yield of form A or N, and σ_2 is the two-photon absorption cross section. Since we collect fluorescence spectrum through a HQ535/50 filter, technically φ_N only comprises a part of fluorescence originating from anionic deprotonated chromophore that appears after the excited-state proton transfer from initially excited neutral form. To obtain the two-photon excitation spectrum in units of molecular brightness, we independently measured ρ_A, φ_A and $\sigma_{2,A}(\lambda)$ of the anionic form in the presence or absence of 5-HT and normalized the unscaled 2PE spectrum to the product $\rho_A\varphi_A\sigma_{2,A}(\lambda)$. The cross section $\sigma_{2,A}(\lambda)$ was measured at the wavelength where the contribution of the neutral form is negligible (λ = 940 nm). This measurement was performed using rhodamine 6G in methanol as a well-characterized reference standard ($\sigma_{2,Rh6G}=9$ GM at 940 nm)[33]. First, spectrally integrated two-photon excited fluorescence signal I was measured as a function of laser power P for both the sample and reference solutions (samples were held in 3 × 3 mm cuvettes (Starna) with maximum optical density < 0.1). The total (spectrally integrated) fluorescence was collected at 90° to excitation laser beam through FF01-770/SP (Semrock) and HQ535/50 (Chroma) filters, using the left emission channel of a PC1 spectrofluorimeter working in photon counting mode. The power dependences of fluorescence were fit to a quadratic function $I=aP^2$, from which the coefficients a_S and a_R were obtained for the sample (index S) and reference (index R) solutions, respectively. Second, the one-photon excited fluorescence signals were measured for the same samples and in the same registration conditions. In this case, a strongly attenuated radiation of a 477-nm line (selected with an interference filter Ealing 35-3565, tilted at 46°) of an IMA101040 ALS (Melles Griot) argon ion laser was used for excitation. The fluorescence power dependences for the sample and reference were measured and fit to a linear function: $I=bP$, from which the coefficients b_S and b_R were obtained. The two-photon absorption cross section was then calculated as follows: $\sigma_{2,S}(\lambda_2)=\frac{a_S}{a_R}\frac{b_R}{b_S}\frac{\varepsilon_S(\lambda_1)}{\varepsilon_R(\lambda_1)}\sigma_{2,R}(\lambda_2)$, where λ_1 is the wavelength used for one-photon excitation (477 nm), λ_2 is the wavelength used for two-photon excitation (940 nm) and $\varepsilon_{R,S}(\lambda_1)$ are the corresponding extinction coefficients, measured at λ_1. This approach allows us to automatically correct for the laser beam properties (pulse duration and spatial intensity distribution), fluorescence collection efficiencies for one- and two-photon modes, photomultiplier tube (PMT) spectral sensitivity, differences in quantum yields and concentrations between S and R solutions. Molecular brightness of the anionic form was then calculated as a product $F_2=\rho_A\varphi_A\sigma_{2,A}(\lambda_m)$ with the 2P cross section taken at spectral maximum, λ_m, for both states of the sensor. The quantum yields, extinction coefficients and fractional concentrations were all determined independently through one-photon measurement. Finally, the two-photon excitation spectra were scaled to the calculated $F_2(940)$ values.

Construction of mammalian expression and viral packaging plasmids. The gene of G-GESS was amplified and used to replace the iGluSnFR gene in pCMV(MinDis).iGluSnFR (ref. [23]). Next, a gene fragment encoding Kir2.1-derived Golgi export trafficking signal (KGC) and ER export signal (ER2) (KGC–ER2) was purchased from Eurofins Genomics and inserted to the C-terminus of the PDGFRβ TM domain, resulting in pDisplay-G-GESS-M for sensor expression at the extracellular surface of mammalian cells. Furthermore, the G-GESS gene fragment fused with the TM domain and KGC–ER2 was amplified from pDisplay-G-GESS and inserted into either pAAV-hSyn-CheRiff-eGFP (ref. [24]) between *Nco*I and *Eco*RI restriction sites for AAV packaging, or pLenti-ReaChR-Citrine (ref. [25]) between *Age*I and *Eco*RI restriction sites for lentiviral packaging. To construct an AAV vector for ratiometric imaging, the pAAV-hSyn-G-GESS-M plasmid was first digested with *Sal*I and *Eco*RI. A gene fragment encoding the TM–KGC–ER2 portion, a P2A self-cleaving peptide and the red fluorescent protein mScarlet-I (ref. [17]) were generated with overlap PCRs and inserted into the pre-digested plasmid via Gibson cloning[34], resulting in pAAV-hSyn-G-GESS-M-mScarlet-I.

Culture and transfection of mammalian cell lines. HEK 293T and SH-SY5Y were purchased from ATCC and MIN6 is a gift from Shuibing Chen (Weill Cornell). HEK 293T and MIN6 cells were cultured as previously described[35]. SH-SY5Y cells were cultured in DMEM/F-12 supplemented with 10% FBS, 100 U ml^{-1} penicillin and 100 μg ml^{-1} streptomycin. All cell lines were incubated at 37 °C in a humidified incubator containing 5% CO_2. At 70–80% confluency, cells were transfected with 2 μg of plasmid DNA and 5 μg of lipofectamine 2000 (Thermo Fisher). Transfected cells were then cultured in complete medium for 24–36 h before imaging.

Culture and transfection of primary neurons. Freshly extracted E18 mouse brain tissue (including the hypothalamus, dorsal raphe, striatum and a part of the cerebellum) was used to prepare dissociated neurons, which were next cultured with 2 ml of NbActiv4 medium (BrainBits) in 35-mm glass-bottom culture dishes pre-coated with poly-D-lysine. Every 2 days, half of the cell culture medium was replaced with fresh NbActiv4. Neurons were transfected on day 7 by following BrainBits's protocol. Briefly, 1 ml of culture medium was taken out from each 35 mm dish and combined with another 1 ml of fresh NbActiv4. The conditioned medium was incubated at 37 °C and 5% CO_2. A total of 4 μg of plasmid DNA and 8 μl of Lipofectamine 2000 (Thermo Fisher) were mixed in 100 μl of BrainBits Transfection Medium and the resultant mixture was incubated at room temperature for 15 min. Next, 1 ml of warm, conditioned NbActiv4 medium was used to replace the medium in each 35 mm dish and the transfection mixture was then added. After 3 h of incubation at 37 °C in a 5% CO_2 incubator, the medium was exchanged again to the conditioned medium. Half of the culture medium was

exchanged every 2 days. Fluorescence imaging was performed between 48 and 72 h after transfection.

Fluorescence imaging of cultured cells. Unless otherwise noted, images were acquired using a 40× oil immersion objective lens on an inverted Leica DMi8 microscope equipped with a Leica SPE-II spectral confocal module and a Photometrics Prime 95B Scientific CMOS camera. The confocal module was used to analyze localization and a 488-nm laser (10 mW) set at ~10% intensity was used to excite G-GESS, and emission was collected at 500–700 nm. Because the brightness of G-GESS in the absence of 5-HT is lower than in the presence of 5-HT, a higher laser intensity (~30%) was used to acquire localization images in the absence of 5-HT. The wide-field Prime 95B camera and a GFP filter cube with a 470/40 nm bandpass excitation filter and a 525/50 nm bandpass emission filter were used for time-lapse imaging. To image the response of G-GESS at the surface of HEK 293T cells to 5-HT, transfected HEK 293T cells were washed three times with Dulbecco's phosphate-buffered saline (DPBS) before imaging. Images were taken before or after addition of serotonin. A similar procedure was used to image the ratiometric response of co-expressed G-GESS-M and mScarlet-I in transfected HEK 293T cells. Images in two channels were acquired sequentially using DMi8 and the SPE-II confocal module. The 488-nm laser (10 mW) was set at 10% intensity and emission was collected at 500–550 nm for the green channel; the 532-nm laser (10 mW) was set at 4% intensity and emission was collected at 580–700 nm for the red channel. To image serotonin release in MIN6 cells, transfected MIN6 cells were thoroughly washed and incubated with Hank's balanced salt solution (HBSS) containing 2.5 mM glucose. After starvation for 40 min, cells were rinsed with fresh HBSS containing 2.5 mM glucose and then retained in the buffer for imaging. Time-lapse images were acquired every 2 s. Following the initial ~30 s of image acquisition, MIN6 cells were stimulated with 25 mM glucose and fluorescence imaging continued for an additional 4.5 min. To image serotonin release in SH-SY5Y cells, transfected SH-SY5Y cells were washed with DPBS three times and then retained in the buffer for imaging. After approximately 1 min of initial acquisition, SH-SY5Y cells were stimulated with 0.1 μM nonivamide and fluorescence imaging continued for an additional 6 min. To image the direct response of G-GESS at the surface of primary neurons to 5-HT, transfected neurons were washed three times with Tyrode's buffer (119 mM NaCl, 2.5 mM KCl, 2 mM $CaCl_2$, 2 mM $MgCl_2$, 25 mM HEPES and 30 mM glucose, pH 7.4) and then retained in the buffer for imaging. Images were taken in the presence or absence of 10 μM serotonin. To image endogenous serotonin release in neurons, an excitatory Tyrode's buffer (32 mM NaCl, 90 mM KCl, 2 mM $CaCl_2$, 2 mM $MgCl_2$, 25 mM HEPES and 30 mM glucose, pH 7.4) was used for stimulation. The photostability and response kinetics of G-GESS was determined on the surface of HEK 293T cells using an upright Scientifica SliceScope Pro 1000 equipped with a Photometrics Prime 95B Scientific CMOS camera and a CoolLed Enhanced pE-300^{white} light-emitting diode (LED) light source. Photostability was examined by time-lapse imaging when excitation light was left continuously on at either 5% or 100% of the overall intensity. Light energy at the focal plan was further determined using a digital optical power meter (Thorlabs, catalog no. PM100D) equipped with a microscope slide photodiode power sensor (Thorlabs, catalog no. S170C). The diameter of the field of view (D_{FOV}) was calculated from the field number (FN) provided by the objective lens manufacturer using the equation: $D_{FOV} = FN/(\text{objective magnification})$. The illumination area was next calculated from $\pi \times (0.5 \times D_{FOV})^2$. Light intensity was then calculated from the total energy divided by the illumination area. To determine the response kinetics, time-lapse imaging was continuously performed with 10 ms exposure and a small amount of 1 μM 5-HT was locally delivered to a cell of interest through a glass micropipette. A Picospritzer II microinjection dispenser was used to deliver the brief, 10-ms puff of 5-HT.

Evaluation of G-GESS-M cytotoxicity in primary mouse neurons. The plate reader-based neurotoxicity assays were adopted from a previous publication[36]. Primary mouse neurons were seeded at a density of 1,000 cells per well in a 96-well glass-bottom plate (Cellvis, catalog no. P96-1.5H-N). Cells were maintained and transfected with either pDisplay-G-GESS-M or pDisplay-sfGFP-M. At 48 h post transfection, wells were randomly assigned into one of the two groups: the first group was treated with 10 μM *tert*-butyl hydroperoxide (tBHP, Sigma-Aldrich catalog no. 458139), while the same volume of ddH_2O was added to the second group of cells. After an additional overnight incubation, the 3-(4,5-dimethylthiazole-2-yl)-2,5-diphenyltetrazolium bromide (MTT) assay (Roche, catalog no. 11465007001) was conducted according to the manufacturer's instructions. Briefly, 10 μl of the MTT labeling reagent was added to each well. The 96-well plate was incubated at 37 °C and 5% CO_2 for 4 h. After incubation, 100 μl of the Solubilization solution was added into each well and incubated overnight at 37 °C and 5% CO_2. Absorbance for each well was next determined at 550 nm using a monochromator-based BioTek Synergy Mx plate reader. Absorbance at 690 nm was also measured and used as the baseline. To further evaluate the impact of G-GESS-M on calcium flux, a calcium mobilization assay was performed on primary mouse neurons in 96-well glass-bottom plates with the GFP-Certified Fluoforte Calcium Assay Kit (Enzo, catalog no. ENZ-51020-KP010) by following the manufacturer's instructions. Briefly, 100 μl of the orange fluorescent dye loading solution was added into each well. Cells were incubated at 37 °C and 5% CO_2 for 45 min. Next, fluorescence was monitored with an interval of 2 s on a CLARIOstar Plus microplate reader (BMG Labtech) by setting excitation at 530 ± 8 nm and emission at 570 ± 8 nm; 100 mM KCl was injected into each well through a reagent dispenser to depolarize neurons.

Preparation of lentivirus and AAV. We followed a protocol provided by Addgene and used the following plasmids (prepared from maxiprep) for lentivirus production: pMD2G, psPAX2 and pLenti-hSyn-G-GESS-M. The viral supernatant was filtered through a 0.45 μm PVDF low protein binding filter unit and further concentrated by PEG-8000 precipitation. Briefly, 4× Lentivirus Concentrator Solution (40% PEG-8000 and 1.2 M NaCl) was mixed with the combined viral supernatant and constantly shaken at 60 r.p.m. and 4 °C for 4 h. The solution was then spun down at 1,600*g* and 4 °C for 60 min. Supernatant was removed without disturbing the pellet, which contains the lentivirus. Next, the viral pellet was thoroughly resuspended with DPBS containing Ca^{2+} and Mg^{2+} at 1/500 of the original supernatant volume. The viral solution was aliquoted, flash frozen and stored at −80 °C. The plasmids (prepared from maxiprep) used in AAV production were as follows: pAdDeltaF6, pAAV2/9n and pAAV-hSyn-G-GESS-M or pAAV-hSyn-G-GESS-M-mScarlet-I. The AAV packing, purification and titering protocol were adopted from Rego et al.[37]. As previously described[38], a cell transduction and fluorescence imaging assay was used to determine viral titers with SH-SY5Y cells. Typical viral titers were 5×10^{11} to 2×10^{12} transduction units (TU) ml^{-1} for AAV and 3×10^{10} to 8×10^{10} TU ml^{-1} for lentivirus.

Preparation, stimulation and imaging of acute brain slices. Intracranial stereotactic injection was used to deliver AAV-hSyn-G-GESS-M or Lenti-hSyn-G-GESS-M virus into the hippocampus of 8 weeks old BALB/cJ mice (The Jackson Laboratory, catalog no. 000651). A total of 3 μl of the virus was injected at a 1 μl min^{-1} flow rate with the following stereotaxic coordinate: from Bregma, AP +1.7 mm, ML +1.2 mm and DV +1.5 mm (ref. [39]) Once injection was completed, the syringe was left in place for 5 min before being retracted. The surgical wound was closed and the animal was left to recover. Three weeks after injection, acute hippocampal slices were prepared for imaging. Freshly extracted mouse brains were sliced into 350 μm thickness in an ice-cold extracellular solution containing 119 mM NaCl, 2.5 mM KCl, 1.3 mM $MgSO_4$, 1 mM NaH_2PO_4, 26 mM $NaHCO_3$, 2 mM $CaCl_2$ and 10 mM glucose. Next, slices were allowed to recover in the aforementioned slicing solution at 34 °C for at least 40 min before being used for experiments. All solutions were continuously bubbled with 95% O_2 and 5% CO_2. A Scientifica SliceScope Pro 1000 equipped with a Photometrics Prime 95B Scientific CMOS camera and a CoolLed Enhanced pE-300^{white} LED light source was used to image evoked serotonin transients in brain slices. The excitation light source was set at 5–10% of the overall intensity and exposure time was set to be 100 ms for initial evaluation of sensor expression and 10 ms for time-lapse imaging. Stimulation pulses were generated in the Axon pClamp10 software with Molecular Devices Axon Digidata 1550B and Multiclamp 700B, followed by further amplification with an Agilent/HP 6824 A to obtain a pulse amplitude of 30 and 50 V. A total of 20 pulses (500 μs per pulse) at frequencies of 8 Hz, 16 Hz, 32 Hz and 64 Hz were used to locally stimulate the hippocampal CA1 region via a cluster bipolar microelectrode (FHC, catalog no. 30209). No obvious difference was observed for brain slices prepared from AAV or lentivirus, so the data were analyzed collectively.

In vivo mouse imaging. Intracranial stereotactic injection was used to deliver Lenti-hSyn-G-GESS-M virus into the PFC of mice. BALB/cJ mice (The Jackson Laboratory, catalog no. 000651, 6–8 weeks of age) were used for imaging drug-induced 5-HT dynamic, whereas C57BL/6J mice (The Jackson Laboratory, catalog no. 000664, 6–8 weeks of age) were used for behavioral experiments. The stereotaxic coordinate for PFC was: from Bregma, AP +2.8 mm, ML +0.5 mm, DV +1.5 mm (ref. [40]). A total of 3 μl of the virus was injected into each mouse at a 0.5 μl min^{-1} flow rate. Once injection was completed, the syringe was left in place for 5 min before being retracted. The surgical wound was closed and the animal was left to recover. One week after viral injection, mice were anesthetized and dexamethasone (Dex, 0.02 ml at 4 mg ml^{-1}) was administered by intramuscular injection to quadriceps to reduce cortical stress responses and cerebral edema. A chronic cranial imaging window made from a 3×3 mm^2 round cover glass (no. 1 thickness) and a 5×5 mm^2 cover glass (no. 1 thickness) was installed according to a previously reported protocol[41]. Mice were allowed to recover for an additional 2 weeks and Dex was administered once daily in the first 7 days after imaging window installation. To perform one-photon imaging, the mouse was lightly anesthetized, head-fixed on a holder, and placed under a Scientifica SliceScope Pro 1000. Imaging sessions started when the mouse was fully awake from the brief anesthesia. Image acquisition was paused briefly for administration of individual drugs, and occasionally a re-adjustment of the microscope focus was needed. MDMA was delivered i.p. at a dose of 10 mg per kilogram of body weight and images were acquired with a 50-ms exposure and 10-s intervals. Flu was delivered i.p. at a dose of 2 mg per kilogram of body weight and images were also acquired with a 50-ms exposure and 10-s intervals. Res was delivered i.p. at a dose of 0.2 mg per kilogram of body weight near the end of the imaging session. To perform the cued

fear conditioning experiment, head-fixed mice acclimated in a dark environment were presented sequentially with a 10-s cue, a 1-s break and a 1-s electric FS (0.6 mA). The cue consists of a 70 dB 5 kHz sine wave tone and a visual stimulation (a bright white screen) delivered with a 7-inch monitor right in front of the mice. The space between the top of the mouse head and the objective lens was wrapped with aluminum foil to minimize light leakage into the imaging system when the visual cue was presented. Images were acquired with a 50-ms exposure every 200 ms.

Ratiometric imaging of 5-HT in mice treated with PCPA. Intracranial stereotactic injection was used to deliver 1 µl of AAV virus (AAV-hSyn-G-GESS-M-mScarlet-I or AAV-hSyn-G-dGESS-M-mScarlet-I) into the hippocampus of 7-week-old BALB/cJ mice (The Jackson Laboratory, catalog no. 000651). The coordinate was: from Bregma, AP +1.7 mm, ML +1.2 mm and DV +1.5 mm (ref.[39]). Seven days post viral injection, PCPA (4-chloro-DL-phenylalanine methyl ester; Sigma-Aldrich, catalog no. C3635) was dissolved in normal saline and delivered into mice via i.p. injection at a dosage of 300 mg kg^{-1} (drug weight per body weight) each day for 5 consecutive days. Brain slices were subsequently prepared and imaged. Mice injected with AAV but untreated with PCPA were used as the control groups. Images were acquired with a Scientifica SliceScope Pro 1000 equipped with a Photometrics Prime 95B Scientific CMOS camera and a CoolLed Enhanced pE-300^{white} LED light source. The excitation intensities for the green and red channels were set at 20% and 15%, respectively. Camera exposure was 10 ms. For each group, five brain slices were obtained from two mice and around seven fluorescent neurons were randomly selected from each slice for data analysis. After subtracting image background with a rolling ball radius of 300 pixels, the fluorescence intensities of each selected neuron in the green and red channels were determined using Fiji (ImageJ) and intensity ratios were calculated.

Data and statistical analysis. Microsoft Excel (v.16.16.27), GraphPad Prism v.9 and Affinity Designer (v.1.8) were used to analyze data and prepare figures for publication. PyMOL (v.2.1.1) was used for structural visualization and analysis. Statistical methods used to determine *P* values are presented in the figure legends and differences with $P < 0.05$ were considered significant. Sample size and the number of replications for experiments are also presented in figure legends. No statistical methods were used to predetermine the sample size. Unless otherwise indicated, data are shown as mean and s.d. Fiji (ImageJ) was used to analyze microscopic images. Imaging background was typically subtracted by setting the rolling ball radius to 300 pixels. Time-lapse images were corrected for motion using the StackReg plugin. Images stacks were corrected for photobleaching by using a linear or exponential decay fitting of baselines. F/F_0 was generated using the 'T-functions' plugin in the 'Cookbook' menu (https://imagej.net/Cookbook) and the processed thresholded images were pseudocolored with a 'Ratio' lookup table.

Reporting Summary. Further information on research design is available in the Nature Research Reporting Summary linked to this article.

Data availability

The gene sequence for G-GESS has been deposited with GenBank under the accession number MW027675. The plasmids for pDisplay-G-GESS-M (plasmid 154273), pAAV-hSyn-G-GESS-M (plasmid 154274), pLenti-hSyn-G-GESS-M (plasmid 154275), pDisplay-G-dGESS-M (plasmid 154276), pAAV-hSyn-G-dGESS-M (plasmid 154277) and pLenti-hSyn-G-GESS-M (plasmid 154278) and their sequence information have been deposited with Addgene. Source data are provided with this paper.

References

23. Marvin, J. S. et al. An optimized fluorescent probe for visualizing glutamate neurotransmission. *Nat. Methods* **10**, 162–170 (2013).
24. Hochbaum, D. R. et al. All-optical electrophysiology in mammalian neurons using engineered microbial rhodopsins. *Nat. Methods* **11**, 825–833 (2014).
25. Lin, J. Y., Knutsen, P. M., Muller, A., Kleinfeld, D. & Tsien, R. Y. ReaChR: a red-shifted variant of channelrhodopsin enables deep transcranial optogenetic excitation. *Nat. Neurosci.* **16**, 1499–1508 (2013).
26. Zhao, Y. et al. An expanded palette of genetically encoded Ca(2)(+) indicators. *Science* **333**, 1888–1891 (2011).
27. Marvin, J. S., Schreiter, E. R., Echevarría, I. M. & Looger, L. L. A genetically encoded, high-signal-to-noise maltose sensor. *Proteins* **79**, 3025–3036 (2011).
28. Chen, S., Chen, Z. J., Ren, W. & Ai, H. W. Reaction-based genetically encoded fluorescent hydrogen sulfide sensors. *J. Am. Chem. Soc.* **134**, 9589–9592 (2012).
29. Fan, Y., Chen, Z. & Ai, H. W. Monitoring redox dynamics in living cells with a redox-sensitive red fluorescent protein. *Anal. Chem.* **87**, 2802–2810 (2015).
30. Kardash, E., Bandemer, J. & Raz, E. Imaging protein activity in live embryos using fluorescence resonance energy transfer biosensors. *Nat. Protoc.* **6**, 1835–1846 (2011).
31. Chen, Z. & Ai, H. W. Single fluorescent protein-based indicators for zinc ion (Zn^{2+}). *Anal. Chem.* **88**, 9029–9036 (2016).
32. Molina, R. S. et al. Understanding the fluorescence change in red genetically encoded calcium ion indicators. *Biophys. J.* **116**, 1873–1886 (2019).
33. Drobizhev, M., Molina, R. S. & Hughes, T. E. Characterizing the two-photon absorption properties of fluorescent molecules in the 680-1300 nm spectral range. *Bio-Protoc.* **10**, e3498 (2020).
34. Gibson, D. G. et al. Enzymatic assembly of DNA molecules up to several hundred kilobases. *Nat. Methods* **6**, 343–345 (2009).
35. Chen, M. et al. Genetically encoded, photostable indicators to image dynamic Zn(2+) secretion of pancreatic islets. *Anal. Chem.* **91**, 12212–12219 (2019).
36. Burroughs, S. L. et al. Plate reader-based assays for measuring cell viability, neuroprotection and calcium in primary neuronal cultures. *J. Neurosci. Methods* **203**, 141–145 (2012).
37. Rego, M. et al. Improved yield of AAV2 and rAAV2-retro serotypes following sugar supplementation during the viral production phase. *bioRxiv* https://doi.org/10.1101/488585 (2018).
38. Ding, B. & Kilpatrick, D. L. Lentiviral vector production, titration, and transduction of primary neurons. *Methods Mol. Biol.* **1018**, 119–131 (2013).
39. Tetteh, H., Lee, J., Lee, J., Kim, J. G. & Yang, S. Investigating long-term synaptic plasticity in interlamellar hippocampus CA1 by electrophysiological field recording. *J. Vis. Exp.* https://doi.org/10.3791/59879 (2019).
40. Otis, J. M. et al. Prefrontal cortex output circuits guide reward seeking through divergent cue encoding. *Nature* **543**, 103–107 (2017).
41. Holtmaat, A. et al. Long-term, high-resolution imaging in the mouse neocortex through a chronic cranial window. *Nat. Protoc.* **4**, 1128–1144 (2009).

Acknowledgements

We thank S. Chen (Weill Cornell) for sharing MIN6 cells, Z. Chen for early exploration of this project, R. Molina for technical help with analyzing two-photon spectra and Y. Wang, Z. Li and other members in the Ai group for helpful discussion and assistance with experiments. Research reported in this publication was supported by funding to H.-w.A. (University of Virginia Start-up Package and NIH grant nos R01 DK122253, R01 GM118675 and R01 GM129291) and to M.D. (NIH grant nos U01 NS094246 and U24 NS109107).

Author contributions

H.-w.A. conceived and supervised the project. X.L. and S. Zhao performed experiments involving brain slices and live mice. M.D. determined photophysical parameters and recorded two-photon excitation spectra. S. Zhang performed all other experiments, including protein engineering, characterization in vitro and in cultured cells, and preparation of viral vectors. All authors analyzed the data and prepared the manuscript.

Competing interests

The authors declare no competing interests.

Additional information

Extended data is available for this paper at https://doi.org/10.1038/s41592-021-01078-7.

Supplementary information The online version contains supplementary material available at https://doi.org/10.1038/s41592-021-01078-7.

Correspondence and requests for materials should be addressed to H.-w.A.

Peer review information *Nature Methods* thanks Bryan Roth, Jing Ren and Oliver Griesbeck for their contribution to the peer review of this work. Nina Vogt was the primary editor on this article and managed its editorial process and peer review in collaboration with the rest of the editorial team.

Reprints and permissions information is available at www.nature.com/reprints.

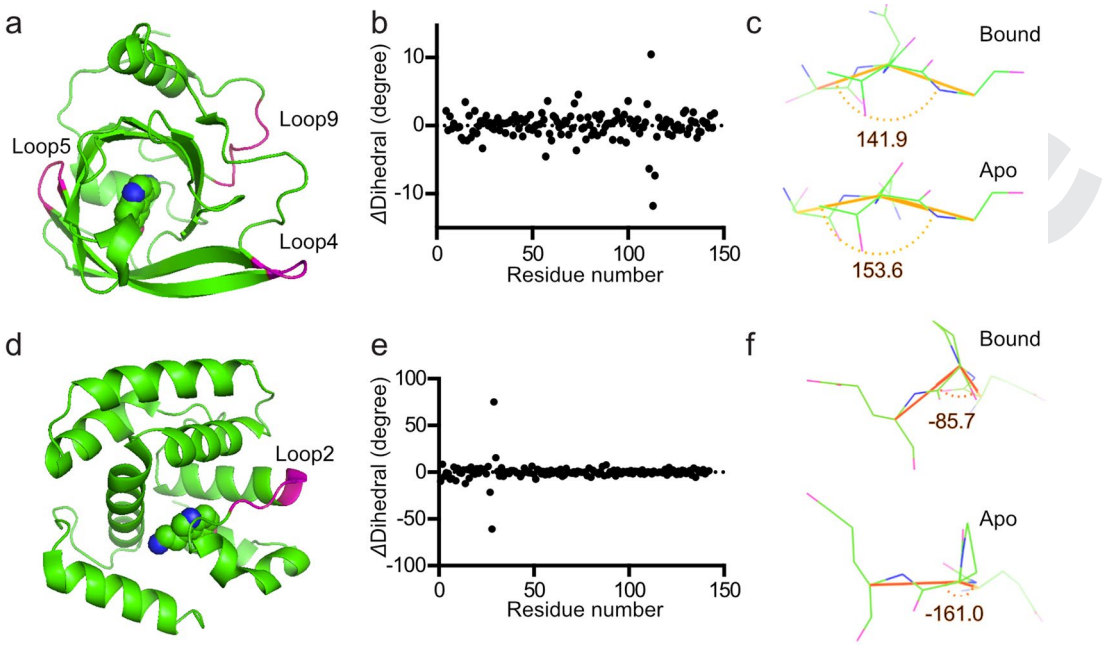

Extended Data Fig. 1 | Structural analysis to identify potential cpGFP insertion sites. a, Cartoon presentation of AM10. Loops showing ligand-dependent changes in dihedral angle (defined by the C_α atoms spanning every four sequential residues) are highlighted in red. **b**, C_α dihedral differences calculated from dihedrals between the ligand-bound (PDB 3BU1) and apo (PDB 3BS2) states of AM10 plotted against residue numbers. **c**, Dihedral angles for residue 113 of AM10 in the ligand-bound and apo states. **d**, Cartoon presentation of D7r4. Loop 2 showing a 5-HT-dependent change in dihedral angle is highlighted in red. **e**, C_α dihedral differences calculated from dihedrals between the ligand-bound (PDB 2QEH) and apo (PDB 2QEV) states of D7r4 plotted against residue numbers. **f**, Dihedral angles for residue 29 of D7r4 in the ligand-bound and apo states.

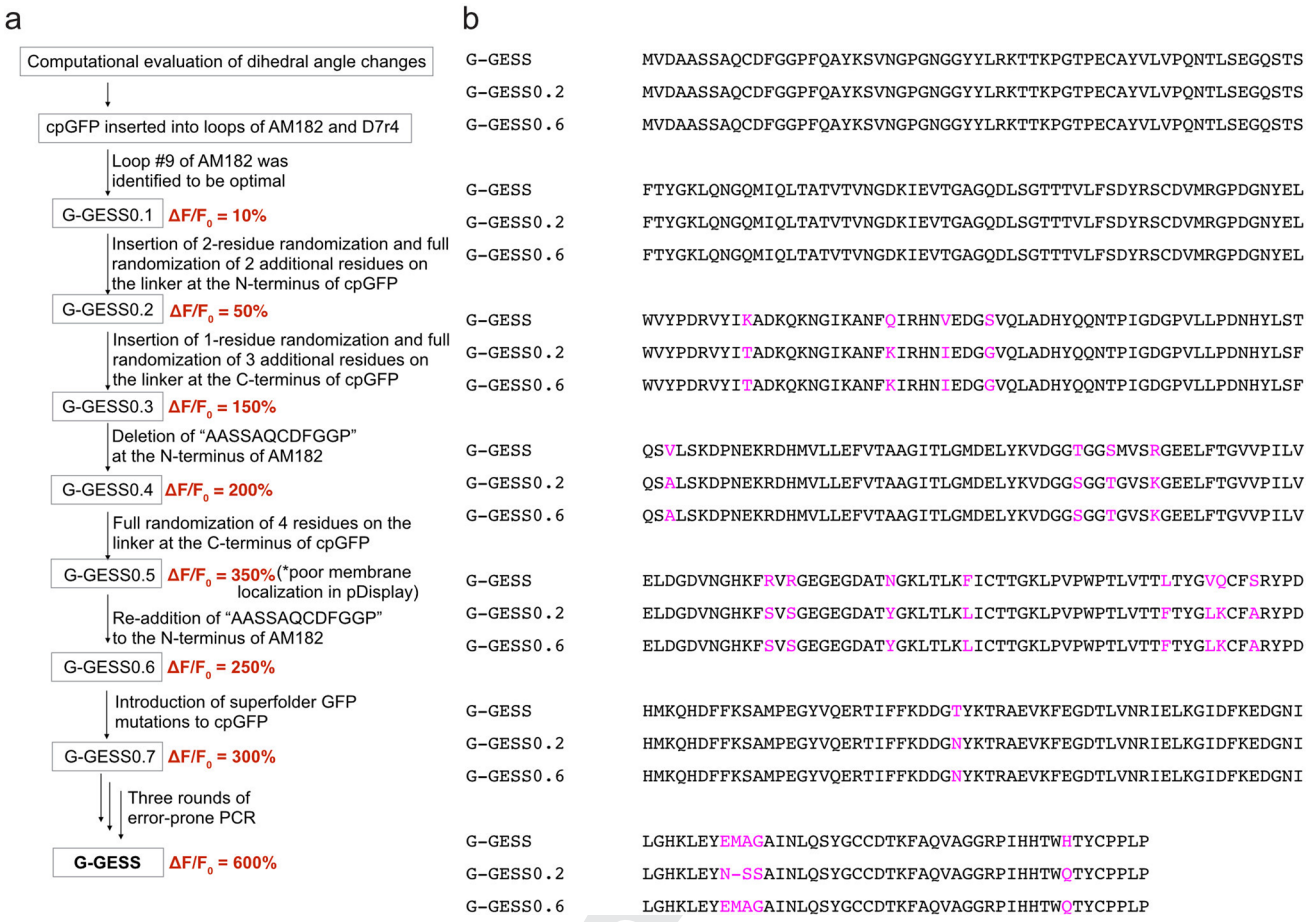

Extended Data Fig. 2 | Process to engineer G-GESS. a, Flowchart to illustrate our integrated, multi-step process to derive G-GESS. $\Delta F/F_0$ for each sensor generation is also presented. From G-GESS0.3 to G-GESS0.4, several N-terminal residues uninvolved in ligand binding were deleted, resulting in increased fluorescence change. However, it was found later in G-GESS0.5 that these residues were important for achieving good cell surface localization, so they were added back to G-GESS0.6. From G-GESS0.6 to G-GESS0.7, superfolder mutations (previously reported for sfGFP) were introduced into the cpGFP fragment of the sensor, resulting in improved brightness and fluorescence change. **b**, Sequence alignment of G-GESS with two earlier variants.

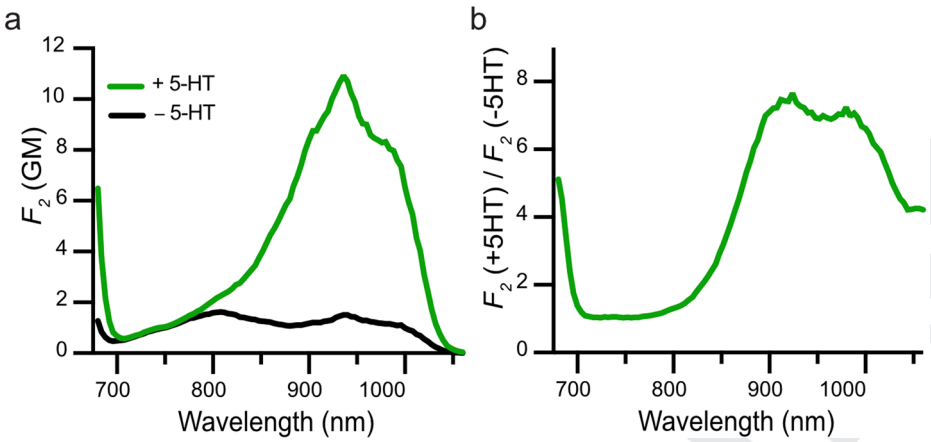

Extended Data Fig. 3 | Two-photon fluorescence characterization of G-GESS. a, Two-photon fluorescence excitation spectra in the presence (green) and absence (black) of 5-HT. **b**, Ratio of two-photon excitation in the presence over absence of 5-HT plotted against wavelength. These experiments were repeated twice with similar results.

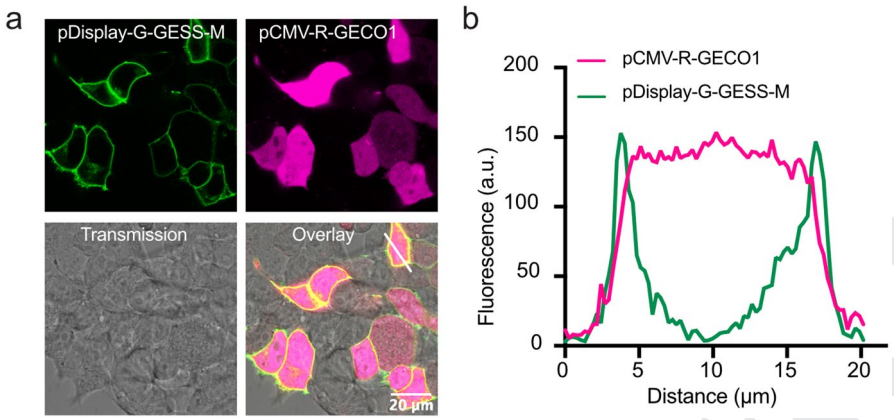

Extended Data Fig. 4 | Characterization of G-GESS-M for membrane localization in HEK 293 T cells. a, Representative fluorescence images of HEK 293 T cells co-transfected with pDisplay-G-GESS-M and pCMV-R-GECO1. Red fluorescent Ca^{2+} sensor R-GECO1 was co-expressed as a whole-cell label. Scale bar, 20 µm. **b**, Fluorescence intensity measured over the white line shown in the 'overlay' image of panel a. These experiments were repeated three times with similar results using independent cultures.

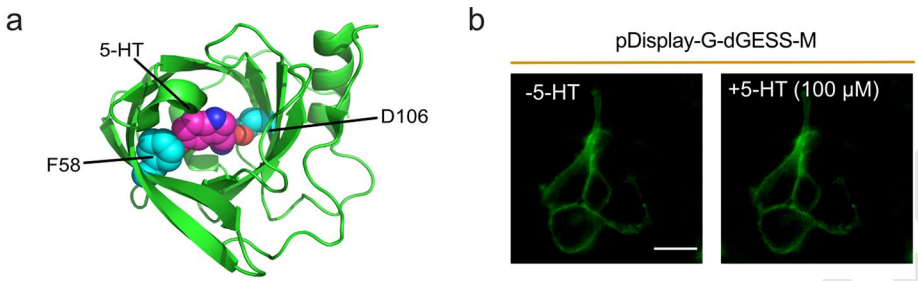

Extended Data Fig. 5 | Construction of G-dGESS, an unresponsive variant of G-GESS. a, Cartoon presentation of AM182 (PDB 3BRN), highlighting the 5-HT ligand (magenta) and two residues (F58 and D106; colored in cyan and numbered according to PDB 3BRN) important for ligand binding. Mutations corresponding to F58A and D106L were introduced into G-GESS to create an unresponsive variant named 'G-dGESS'. **b**, Representative fluorescence images of G-dGESS-M at the surface of HEK 293 T cells, in the presence or absence of 5-HT. This experiment was repeated three times with similar results using independent cell cultures. Scale bar, 20 µm.

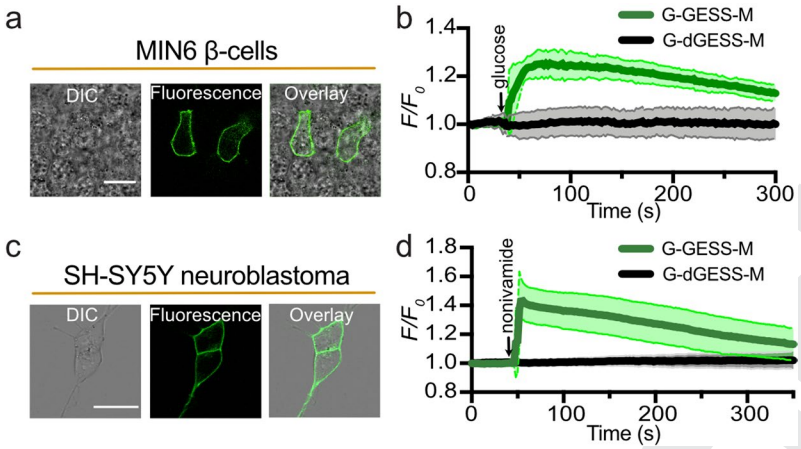

Extended Data Fig. 6 | Imaging of 5-HT release from β-cells and neuroblastoma cells. a, Representative images of G-GESS-M at the surface of mouse pancreatic MIN6 β-cells. Scale bar, 20 μm. **b**, Fluorescence traces of G-GESS-M in response to high glucose (25 mM). n = 7 cells for G-GESS-M and 6 cells for G-dGESS-M from 3 independent repeats. **c**, Representative images of G-GESS-M at the surface of SH-SY5Y neuroblastoma cells. Scale bar, 20 μm. **d**, Fluorescence traces of G-GESS-M in response to nonivamide (0.1 μM). n = 13 cells from 3 repeats for each group. Data are presented as mean ± s.d. of indicated replicates.

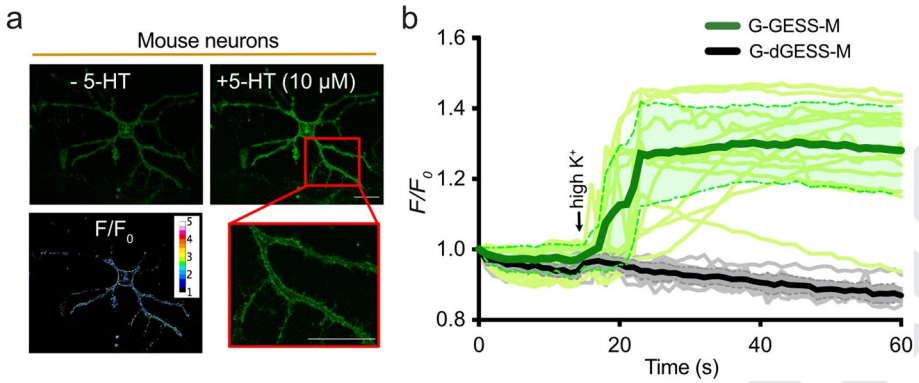

Extended Data Fig. 7 | Imaging of 5-HT release in primary mouse neuron cultures. a, Representative images of G-GESS-M at the surface of primary mouse neurons in response to 5-HT (10 µM). Also shown is a pseudocolor ratiometric image of the neuron in the presence over absence of 5-HT. Scale bar, 20 µm. This experiment was repeated three times with similar results using independent cultures. **b**, Fluorescence traces of G-GESS-M at the surface of primary mouse neurons, in response to high potassium induced membrane polarization. n = 19 cells for G-GESS-M and 12 cells for G-dGESS-M from 4 repeats. Data are presented as mean ± s.d. overlaid on the top of the traces of individual cells.

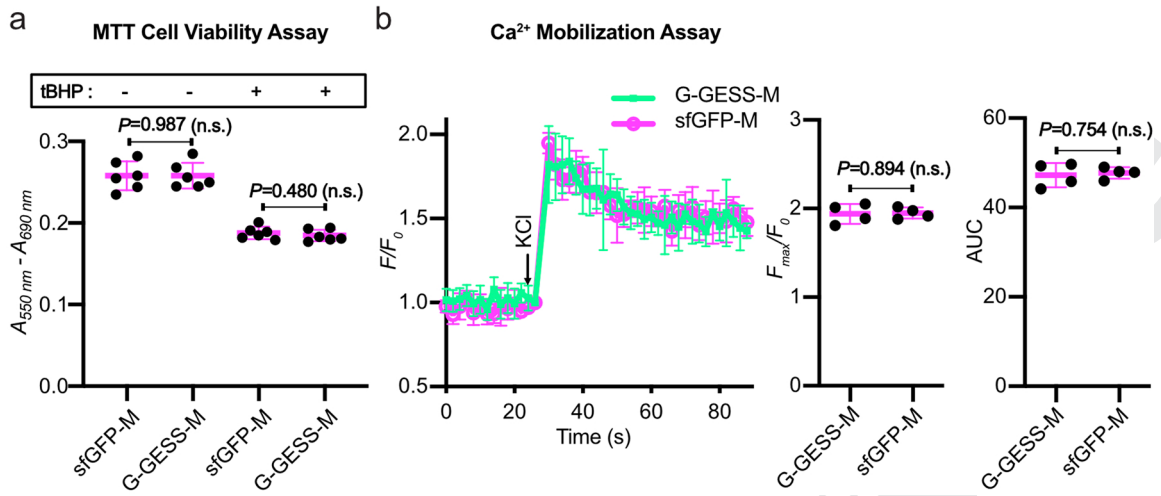

Extended Data Fig. 8 | Evaluation of G-GESS-M cytotoxicity in primary mouse neurons. a, MTT assay of primary neurons transfected with pDisplay-G-GESS-M or pDisplay-sfGFP-M in the absence or presence of the oxidative stress inducer, *tert*-butyl hydroperoxide (tBHP). *P* values determined by unpaired, two-tailed Student's *t*-test. n = 6 cultures each group. **b**, Ca^{2+} mobilization assay of primary neurons transfected with pDisplay-G-GESS-M or pDisplay-sfGFP-M in response to depolarization with 100 mM KCl at the indicated time point. Intracellular Ca^{2+} was monitored with an orange fluorescent Ca^{2+} indicator (Enzo GFP-Certified Fluoforte Calcium Assay Kit). *P* values determined by unpaired, two-tailed Student's *t*-test. n = 4 cultures each group. Individual data points and mean ± s.d. are presented. n.s., not significant.

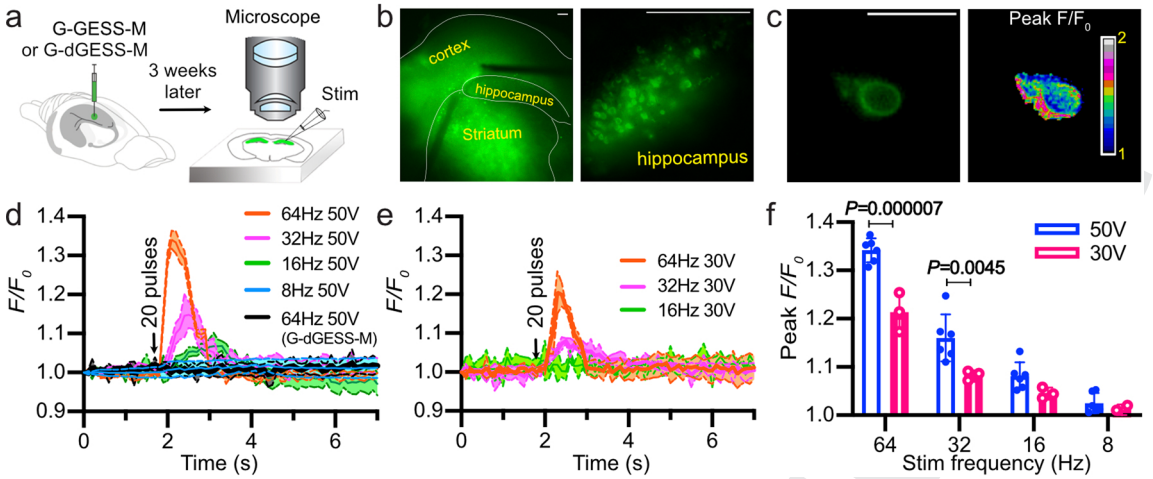

Extended Data Fig. 9 | Imaging of 5-HT release in acute mouse brain slices. a, Schematic diagram illustrating the preparation of acute mouse brain slices with viral expression of G-GESS-M. **b**, Representative fluorescence images of G-GESS-M-expressing mouse brain slices. Scale bar, 200 μm. This experiment was repeated five times with three slice preparations and similar results were obtained. **c**, Representative fluorescence images of G-GESS-M-expressing hippocampal neurons in mouse brain slices in response to electrical stimuli (20 pulses at 64 Hz). Also shown is a pseudocolor ratiometric image (peak F/F_0) of a representative neuron. Scale bar, 20 μm. This experiment was repeated six times with three slice preparations and similar results were obtained. **d**, Fluorescence traces of G-GESS-M in response to 20 pulses of electric stimuli at 50 V and the indicated frequencies. **e**, Fluorescence traces of G-GESS-M in response to 20 pulses of electric stimuli at 30 V and the indicated frequencies. **f**, Maximal fluorescence ratio change (peak F/F_0) plotted against stimulation frequency at 50 V or 30 V. *P* values determined by 2-way ANOVA with Sidak's multiple comparisons test. n = 6 cells on 3 slices from 2 mice for each group stimulated at 50 V, and 3 cells on 2 slices from 2 mice for each group stimulated at 30 V. Data are presented as mean ± s.d in all panels.

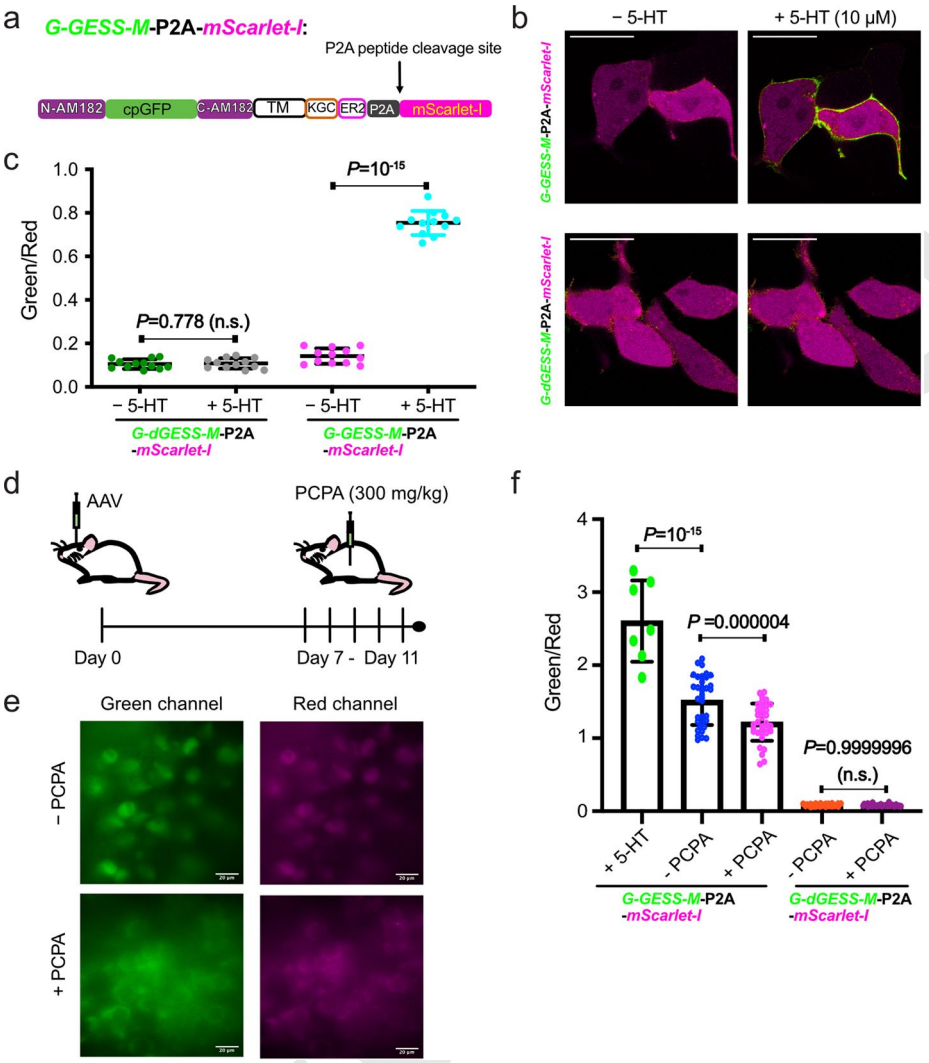

Extended Data Fig. 10 | Bicistronic co-expression of G-GESS-M with a red fluorescent protein mScarlet-I to detect pharmacological modulation of 5-HT by p-chlorophenylalanine methyl ester (PCPA), a tryptophan hydroxylase inhibitor. a, Schematic diagram illustrating the co-expression construct including G-GESS-M, a P2A peptide self-cleaving site, and mScarlet-I. **b**, Representative fluorescence images of the co-expression construct expressed in HEK 293 T cells in the absence and presence of 5-HT acquired with a Leica DMi8 SPE confocal microscope. Scale bar, 20 μm. **c**, Quantitative analysis of the green-to-red intensity ratios of HEK 293 T cells, in the absence or presence of 5-HT for G-dGESS-M-P2A-mScarlet-I and G-GESS-M-P2A-mScarlet-I. *P* values determined by unpaired, two-tailed Student's *t*-test. n = 12 random cells from three independent cultures. **d**, Schematic diagram illustrating the mouse treatment timeline, including intracranial injection of AAV on Day 0 and PCPA injection from Day 7 to Day 11. Acute brain slices were prepared and imaged on Day 12. **e**, Representative fluorescence images of the co-expression construct expressed in the hippocampus of mice with or without PCPA treatment. Images were acquired with a Scientifica SliceScope Pro 1000. Scale bar, 20 μm. **f**, Quantitative analysis of the green-to-red intensity ratios of mouse brain slices, in the presence or absence of PCPA. *P* values determined by one-way ANOVA with Tukey's multiple comparisons test. n = 7 cells on one 5-HT-treated slice expressing G-GESS-M-P2A-mScarlet-I, and 35 cells on 5 slices from two mice for all other groups. Individual data points and mean ± s.d. are presented. n.s., not significant.

nature research

Corresponding author(s): Hui-wang Ai

Last updated by author(s): Dec 17, 2020

Reporting Summary

Nature Research wishes to improve the reproducibility of the work that we publish. This form provides structure for consistency and transparency in reporting. For further information on Nature Research policies, see Authors & Referees and the Editorial Policy Checklist.

Statistics

For all statistical analyses, confirm that the following items are present in the figure legend, table legend, main text, or Methods section.

n/a	Confirmed	
☐	☒	The exact sample size (*n*) for each experimental group/condition, given as a discrete number and unit of measurement
☐	☒	A statement on whether measurements were taken from distinct samples or whether the same sample was measured repeatedly
☐	☒	The statistical test(s) used AND whether they are one- or two-sided *Only common tests should be described solely by name; describe more complex techniques in the Methods section.*
☒	☐	A description of all covariates tested
☒	☐	A description of any assumptions or corrections, such as tests of normality and adjustment for multiple comparisons
☐	☒	A full description of the statistical parameters including central tendency (e.g. means) or other basic estimates (e.g. regression coefficient) AND variation (e.g. standard deviation) or associated estimates of uncertainty (e.g. confidence intervals)
☐	☒	For null hypothesis testing, the test statistic (e.g. *F*, *t*, *r*) with confidence intervals, effect sizes, degrees of freedom and *P* value noted *Give P values as exact values whenever suitable.*
☒	☐	For Bayesian analysis, information on the choice of priors and Markov chain Monte Carlo settings
☒	☐	For hierarchical and complex designs, identification of the appropriate level for tests and full reporting of outcomes
☒	☐	Estimates of effect sizes (e.g. Cohen's *d*, Pearson's *r*), indicating how they were calculated

Our web collection on statistics for biologists contains articles on many of the points above.

Software and code

Policy information about availability of computer code

Data collection	Leica LAS X (Version 3.5.7) or Micro-Manager (Version 1.14) were used to collect microscopic images. BioTek Gen5 or BMG LABTECH CLARIOstar Plus Reader Control and Data Analysis Software were used for fluorescence measurements. Axon pClamp10 was used to generate stimulation pulses. See Methods for additional information.
Data analysis	Fiji was used to analyze microscopic images. Microsoft Excel (Version 16.16.27), OriginPro 8, GraphPad Prism 9, and Affinity Designer (Version 1.8) were used to analyze data and prepare figures for publication. PyMOL (Version 2.1.1) was used for structural visualization and analysis. See Methods, "Data and Statistical Analysis" subsection for additional information.

For manuscripts utilizing custom algorithms or software that are central to the research but not yet described in published literature, software must be made available to editors/reviewers. We strongly encourage code deposition in a community repository (e.g. GitHub). See the Nature Research guidelines for submitting code & software for further information.

Data

Policy information about availability of data

All manuscripts must include a data availability statement. This statement should provide the following information, where applicable:

- Accession codes, unique identifiers, or web links for publicly available datasets
- A list of figures that have associated raw data
- A description of any restrictions on data availability

The gene sequence for G-GESS has been deposited to GenBank under the accession number MW027675. The plasmids for pmDisplay-G-GESS (Plasmid #154273), pAAV-hSyn-G-GESS (Plasmid #154274), pLenti-hSyn-G-GESS (Plasmid #154275), pmDisplay-G-dGESS (Plasmid #154276), pAAV-hSyn-G-dGESS (Plasmid #154277), and pLenti-hSyn-G-GESS (Plasmid #154278) and their sequence information have been deposited to Addgene. Additional data are available from the corresponding author upon request.

Field-specific reporting

Please select the one below that is the best fit for your research. If you are not sure, read the appropriate sections before making your selection.

☒ Life sciences ☐ Behavioural & social sciences ☐ Ecological, evolutionary & environmental sciences

For a reference copy of the document with all sections, see nature.com/documents/nr-reporting-summary-flat.pdf

Life sciences study design

All studies must disclose on these points even when the disclosure is negative.

Sample size	No statistical methods were used to predetermine sample size. Sample sizes are indicated for each experiment and were chosen based on similar studies. Experiments were performed in triplicates unless otherwise noted.
Data exclusions	No data was excluded from data analysis for in vitro assays. In vivo data were excluded when no fluorescence was observed or some animals were euthanized before completion of all experiments (due to reasons such as Covid-19 shutdown or animal health conditions).
Replication	Replication information for all data reported in this study is stated in figure legends. All repetitions were deemed successful.
Randomization	Cell cultures and mice were randomly assigned to treatment groups.
Blinding	Blinding was not used and is not necessary for sensor development and in vitro characterization experiments, because the screening and characterization were based on subjective values. For in vivo behavioral experiments, the investigator who acquired and analyzed the data was blinded to the group allocation during experiments.

Reporting for specific materials, systems and methods

We require information from authors about some types of materials, experimental systems and methods used in many studies. Here, indicate whether each material, system or method listed is relevant to your study. If you are not sure if a list item applies to your research, read the appropriate section before selecting a response.

Materials & experimental systems

n/a	Involved in the study
☒	☐ Antibodies
☐	☒ Eukaryotic cell lines
☒	☐ Palaeontology
☐	☒ Animals and other organisms
☒	☐ Human research participants
☒	☐ Clinical data

Methods

n/a	Involved in the study
☒	☐ ChIP-seq
☒	☐ Flow cytometry
☒	☐ MRI-based neuroimaging

Eukaryotic cell lines

Policy information about cell lines

Cell line source(s)	MIN6 cells was a gift from Dr. Shuibing Chen at Weill Cornell Medical College. HEK 293T cells and SH-SY5Y cells were purchased from ATCC.
Authentication	Not authenticated in our lab, but HEK and SH-SY5Y were directly purchased from ATCC (authenticated using short tandem repeat per the vendor).
Mycoplasma contamination	Cells were routinely tested for mycoplasma (every 2-3 months) and were always negative.
Commonly misidentified lines (See ICLAC register)	None of the cell lines used are listed in the current ICLAC database.

Animals and other organisms

Policy information about studies involving animals; ARRIVE guidelines recommended for reporting animal research

Laboratory animals	BALB/cJ mice (The Jackson Laboratory, Cat. #000651, 6-8 weeks of age) and C57BL/6J mice (The Jackson Laboratory, Cat. #000664, 6-8 weeks of age) of both sex were used. All mice were hosted in a temperature controlled room (~ 23°C) with a 12h/12h dark-light cycle and ~ 50% humidity.

Wild animals	This study didn't involve wild animal.
Field-collected samples	This study didn't involve field-collected samples.
Ethics oversight	All animal procedures were conducted in accordance with the protocol approved by the Animal Care and Use Committee at the University of Virginia.

Note that full information on the approval of the study protocol must also be provided in the manuscript.